Journal of Nanobiotechnology

RESEARCH Open Access

Carbon dots-facilitated on-demand dissolution of Ca-alginate hydrogel *via* site-specific mineralization for wound healing

Qian Li[1,3], Chenguang Liu[2*] and Dongming Xing[1,3,4*]

Abstract

On-demand dissolution of hydrogels has shown much potential in easy and pain-free removal of wound dressings. This work firstly describes a type of carbon dots (CDs) for dissolving Ca-alginate hydrogel *via* site-specific mineralization method. The CDs were characterized by two features, which included presence of primary/secondary amine groups and generation of calcium crystals with Ca^{2+}. Especially, the amount of primary/secondary amine groups on CDs played key role in determining whether hydrogel could be dissolved. When there were sufficient primary/secondary amine groups, the mineralization occurred on CDs rather than alginates due to the hydrogen bond between primary/secondary amine and carboxyl of alginates. Thereby, this promoted the gel-sol transition through Ca^{2+} capture from the hydrogels. Moreover, antibacterial test revealed Ca^{2+} capture from cell walls, while in vivo test revealed hypoxia relief due to porous structures of the renewed hydrogels. Overall, CDs with sufficient primary/secondary amine groups could dissolve Ca-alginate hydrogel through site-specific mineralization method, accompanying by additional functions of antibacterial and hypoxia relief.

Keywords Carbon dot, Mineralization, Alginate hydrogel, On-demand dissolution

Introduction

According to the World Health Organization, burn is the fourth most devastating injury in the world and approximately 11 million people require medical attention each year [1, 2]. Burn, as damage of the skin, is commonly caused by excessive heat or caustic chemicals. Wound dressing plays a key role in promoting timely and healthy wound healing through absorbing wound exudates and protecting the wound site from external environment [3, 4]. Traditional cotton-based wound dressings are most commonly used [1]. However, they tend to adhere to wound beds and cause additional trauma and pain during dressing changes [2, 5, 6]. In fact, the pain can be severe enough to require anesthesia.

To achieve easy and painless wound dressing changes, hydrogels possessing the ability to dissolve on-demand have aroused much attention in the last decade. Breakable chemical and physical crosslinks have been used to prepare dissolvable hydrogels. Chemically crosslinked hydrogels are mainly dissolved through reactions such as thiol-thioester exchange, thiol-disulfide exchange, thiol-diselenide exchange and thiol-carbonate bonds exchange [7–11]. These hydrogels have been prepared from functional molecules such as thioester-containing aldehyde-terminated 4-arm polyethylene glycol [8], cystamine-modified hyaluronic acid [9], chitosan modified γ-selenobutyrolactone [10] and aldehyde modified block

*Correspondence:
Chenguang Liu
liucg@ouc.edu.cn
Dongming Xing
xdm@qdu.edu.cn

Full list of author information is available at the end of the article

© The Author(s) 2024. **Open Access** This article is licensed under a Creative Commons Attribution-NonCommercial-NoDerivatives 4.0 International License, which permits any non-commercial use, sharing, distribution and reproduction in any medium or format, as long as you give appropriate credit to the original author(s) and the source, provide a link to the Creative Commons licence, and indicate if you modified the licensed material. You do not have permission under this licence to share adapted material derived from this article or parts of it.The images or other third party material in this article are included in the article's Creative Commons licence, unless indicated otherwise in a credit line to the material. If material is not included in the article's Creative Commons licence and your intended use is not permitted by statutory regulation or exceeds the permitted use, you will need to obtain permission directly from the copyright holder.To view a copy of this licence, visit http://creativecommons.org/licenses/by-nc-nd/4.0/.

Graphical Abstract

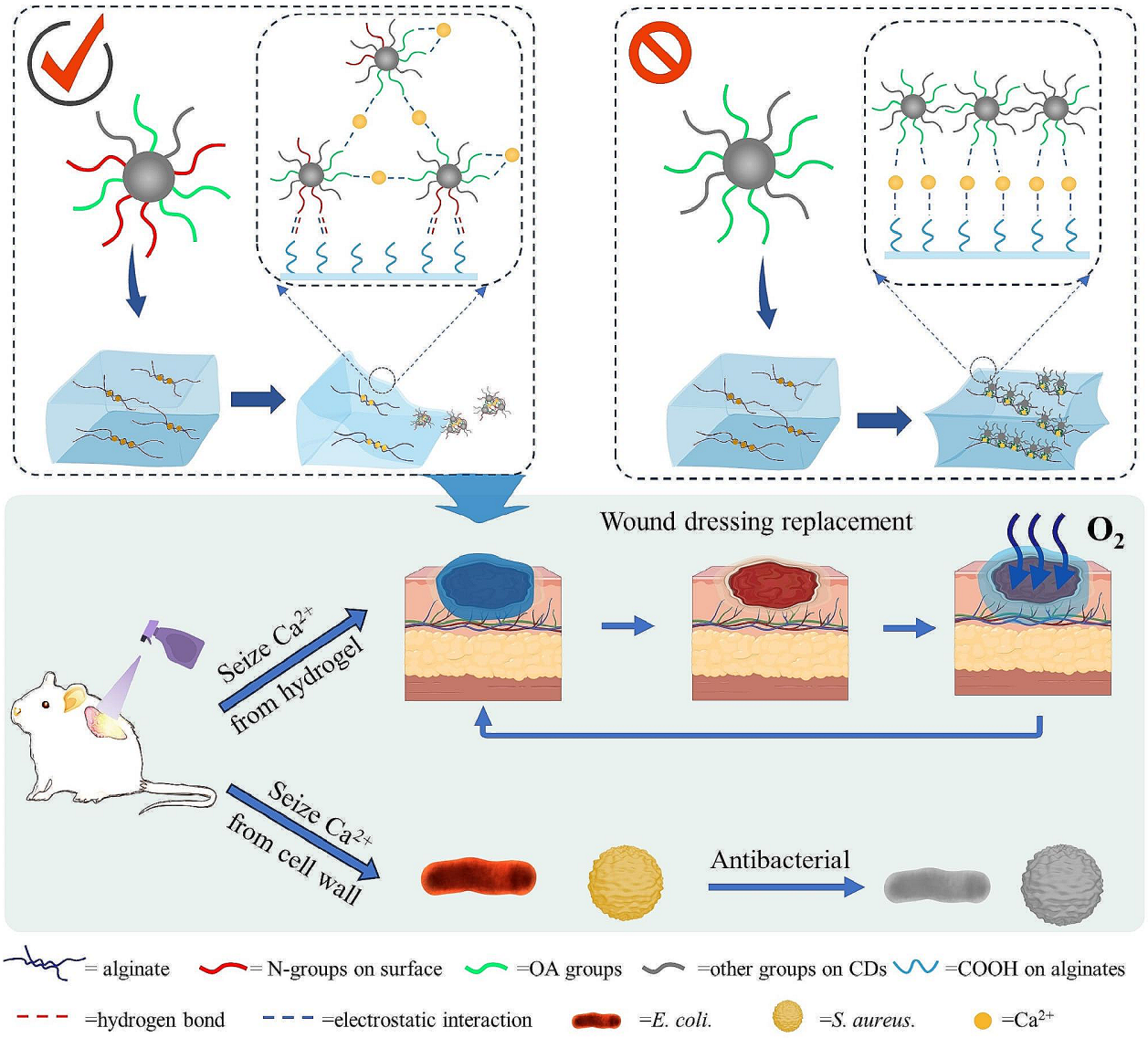

copolymer containing carbonate bonds [11]. Physically crosslinked hydrogels are mainly dissolved by breakage of non-covalent interactions such as H-bonding, host-guest interaction and electrostatic interaction [5, 12, 13]. For example, Gokaltun et al. prepared supramolecular hybrid hydrogel using acrylamide-random-[3-(methacryloylamino) propyl] trimethylammonium chloride, cucurbit uril and anionic polymer-coating clay nanosheets [5]. The above methods are focused on design and syntheses of constituent molecules of hydrogels, however, molecular syntheses may involve complicated chemical processes and toxic compounds. The complicated chemical processes could cause unfavorable influence for large-scale production, while toxic compounds at levels higher than can be supported by safety data may be harm to the human body [5, 14].

On the flip side, syntheses of dissolving agents may be a promising alternative for gel-sol transition. Alginate hydrogel, which has been approved by the Food and Drug Administration (FDA), has been considered as a preferable wound dressing due to its ability to maintain moisture, hemostatic effect, excellent biocompatibility, low toxicity, in-situ and fast formation [15–17]. The sol-gel transition of alginate solution has been quite clear after many years of investigation. It occurs by complex binding with multivalent cations (except for Mg^{2+}) under mild conditions. However, the gel-sol transition of alginate hydrogel just come forth in recent years. Dissolvable

Cu-alginate hydrogel has been reported by our group for burn wound treatment. Cu^{2+} was seized from Cu-alginate hydrogel through competitive complexation [18]. However, high concentration of Cu^{2+} in hydrogels could cause damage to the cells involved in the wound healing process [19]. Ca^{2+} cross-linked alginate hydrogel without any toxicity is by far the most commonly used alginate hydrogel for wound healing treatment. Therefore, there is a compelling need to dissolve Ca-alginate hydrogels.

Mineralization, which takes place under mild chemical conditions, has been reported as a crystallization pathway describing the movement of ions from the sources to the final products [20, 21]. Complex calcium in Ca-alginate hydrogels can be transformed into calcium deposits under the modulation of organic substances such as proteins, amino acids and carbohydrates. Ca^{2+} binds to anions such as carboxyl groups of alginates, oxalate and carbonate in the early stage of mineralization. However, the binding of Ca^{2+} with carboxyl groups of alginates would cause mineralization of alginates and block gel-sol transition of alginate hydrogel. Breaking the interaction between Ca^{2+} and alginates may prevent the mineralization of alginates. As strong interaction exists between nitrogenous groups and carboxyl groups, we proposed excessive nitrogenous groups entering into surface of alginates wound prevent mineralization of alginates through competitively binding to alginates.

Carbon dots (CDs) were chosen to prove this hypothesis, for their ability to act as mineralization templates in a fashion similar to organic molecules [22–24]. Several kinds of amino acids or polyethyleneimine (PEI) were chosen as nitrogen sources. To add function of generating calcium precipitations with Ca^{2+}, oxalic acid (OA) was chosen as the other starting material. The effect of types and amounts of N-groups on dissolution of Ca-alginate hydrogels was analyzed. The cytotoxicity and antibacterial activity of CDs were characterized, and the therapeutic potential was investigated in a burning wound model.

Materials and methods

Materials

Lysine (Lys), aspartate (Asp), serine (Ser), histidine (His), arginine (Arg), proline (Pro), oxalic acid (OA), polyethyleneimine (PEI, MW = 1800), $CaCl_2$, $CuCl_2$, $FeCl_3$ and $AlCl_3$ were supplied by Shanghai Aladdin Co. Ltd (China). Sodium alginate (SA, 200 mPa·s) and $ZnSO_4$ were obtained from Shanghai Macklin Biochemical Co. Ldt (China). CCK-8 kit were purchased from Beyotime Institute of Biotechnology (Shanghai, China). Fetal bovine serum (FBS) and Dulbecco's modified Eagle's medium (DMEM) were obtained from Gibco Co. Ltd. Deionized water was used in all the experiments.

Synthesis of CDs

CDs with diverse mineralization properties were synthesized using oxalic acid and different nitrogenous compounds (N-compounds). After dissolving certain amounts of oxalic acid and N-compounds into 10 mL distilled water (Table S1), the mixture was transferred into 25 mL Teflon-lined stainless-steel autoclave and heated to 150 °C for 7 h. The resulting solution was purified by centrifugation at 4000 rpm and dialyzed using 100–500 molecular-weight-cutoff bag. After lyophilizing certain volume of CDs, dry CDs were weighted for calculating concentration of CDs. CDs were named based on the type of N-compounds and mass ratio of oxalic acid to total weights. CD_n, CD_{n+Ser}, CD_{n+Asp}, CD_{n+Arg}, CD_{n+His}, CD_{n+Pro}, CD_{n+PEI} represented CDs prepared from lysine, serine, aspartate, arginine, histidine, proline and PEI, respectively. Subscript n (n = 0, 1/9, 1/4, 1/2, 3/4 or 1) represented mass ratio of oxalic acid to total weights.

Characterization of CDs

Surface groups were investigated using Fourier transform infrared (FTIR) spectroscopy (Nicolet, USA). Elemental composition was investigated by X-ray photoelectron spectroscopy (XPS, Thermal Electron, USA). The UV-Vis absorption and fluorescence spectra were recorded on UV-1900 spectrophotometer (Shimadzu Co., Japan) and RF-6000 fluorescence spectrometer (Shimadzu, Japan), respectively.

Preparation and dissolution of alginate hydrogels

Alginate hydrogel was prepared by the ionic gelation method. In brief, 12 mg/mL SA solution was added into vial or wound, and then 0.1 M metal ion solution was added or sprayed until formation of metal-alginate hydrogel.

After putting hydrogel in room for 4 days, CD aqueous solution after dialysis mentioned above was sprayed onto hydrogels (equivalent 0.25 g CDs per g of hydrogel) and incubated at 25 ℃ for gel-sol transition. The dissolved hydrogel was centrifugated, dialyzed and weighted to calculate the ratio of dissolution. Microstructure of the hydrogels were measured by scanning electron microscopy (SEM; JEOL, Japan) equipped with energy-dispersive X-ray (EDX) spectrometer. To study whether alginate participated in mineralization process of $CD_{1/4}$, the dissolved suspension was centrifugated to separate calcium precipitations. Then, the supernatant and sedimentation were investigated by FTIR after lyophilization.

Swelling of hydrogels

In order to measure the swelling of hydrogels during dissolution, the hydrogels were treated with $CD_{1/4}$ and sampled at different time intervals. Then, undissolved hydrogels were washed with distilled water, 0.3 M NaCl

solution and distilled water subsequently. The mass of the hydrogel was measured before and after lyophilization. Formula (1) was used to describe the swelling of hydrogel.

$$Swelling = (W_B - W_A)/W_A \times 100\% \quad (1)$$

where W_B and W_A are the hydrogel weight before and after lyophilization, respectively.

Rheological measurement

The rheological measurements were obtained on rheometer (Anton Paar, Austria). A time sweep test with a strain of 1% and an angular frequency of 10 rad/s was employed to follow the degradation process. The measurement was performed with a swollen hydrogel between preheated rheometer plates and $CD_{1/4}$ solution.

Cytotoxicity test

The cell viability was evaluated using CCK-8 assay on L929 mouse fibroblast cells according to previous reports [18]. All materials and solutions for this experiment were sterilized by 0.22 μm filter. For measuring the cytotoxicity of CDs, CDs were dissolved in PBS and incubated with cells for 90 min. After washing with PBS, cells were cultured in DMEM for another 12 h. The cell viability of hydrogel before and after dissolution was measured by incubating hydrogel extract or dissolved hydrogel solution with cells for 24 h, respectively. To obtain hydrogel extract and dissolved hydrogel solution, freeze-dried hydrogel before and after gel-sol transition were incubated in DMEM for 48 h, respectively. Finally, cells were treated with CCK-8 and the absorbance was measured at 450 nm.

Antibacterial activity

The growth inhibition effect of carbon dots was determined on *E. coli* and *S. aureus.* Generally, the strains at a level of 3.0 Log CFU/mL were incubated with $CD_{1/4}$, and the turbidity of the medium liquid at 570 nm was measured at time points during bacteria growth. The same amount of sterile water was taken as the control.

In order to determine the morphological changes of bacteria cells after $CD_{1/4}$ treatment, TEM analysis was performed. The treatment was the same as mentioned in the growth inhibition assay. After being treated by $CD_{1/4}$ for 50 min, the bacteria cells were centrifuged at 8,000 g for 10 min, washed with PBS and fixed in 2.5% glutaraldehyde overnight at 4 °C. Then the bacteria cells were examined by TEM.

Wound healing treatment

All animal experiments were approved by the Institutional Animal Care and Use Committee of Affiliated Hospital of Qingdao University. After anesthetizing with pentobarbital sodium, Sprague-Dawley male rats (SD rats, 6–8 weeks) were depilated on the back using an electric clipper. Burns with a radius of 1.5 cm were created using preheated soldering iron at 100 ℃ for 16 s. The SD rats were randomly divided into control group, hydrogel group and hydrogel+$CD_{1/4}$ group. For hydrogel+$CD_{1/4}$ group, the hydrogel was replaced every four days. $CD_{1/4}$ solution (18 mg/mL) was sprayed onto Ca-alginate hydrogel and incubated for about 50 min.

For histological and histochemical analysis, the skin tissues were collected on day 16. Tissues were fixed with paraformaldehyde, embedded in paraffin and cut into 5 μm slices. After the slices were stained with hematoxylin and eosin (H&E), Masson's trichrome or CD68/HIF-1α monoclonal antibody, images were recorded by a light microscope.

Statistical analysis

Data were shown as mean±standard deviation. One-way ANOVA followed by Tukey's post-hoc test was used to assess significance. The $^{*}p<0.05$, $^{**}p<0.01$ and $^{***}p<0.001$ were considered as statistically significant difference.

Results and discussion

Synthesis and characterization of CDs

As shown in Fig. 1A and Figure S1, the formed $CD_{1/4}$ with the best dissolving effect was spherical in shape with average diameter of 2.48±0.41 nm and well dispersed from each other. After lyophilization, $CD_{1/4}$ was re-dissolved in distilled water. Figure S1 also showed the particle size was still relatively small (2.62±0.56 nm), which indicated good redispersion of $CD_{1/4}$. CD_0, $CD_{1/9}$ and $CD_{1/4}$ had relatively high absorption around 340 nm, which could be attributed to the formation of defect surface states induced by the N heteroatoms (Fig. 1B) [25]. However, this peak sharply decreased in $CD_{1/2}$, $CD_{3/4}$ and CD_1, indicating reduction of nitrogen-related defect surface states. The fluorescence spectrum revealed both fluorescence intensity and peak position of $CD_{1/4}$ were dependent on the excitation wavelength (Figure S2). The FTIR spectra show the characteristic peaks of CDs (Fig. 1C). The peak at 1534 cm^{-1} in lysine, CD_0, $CD_{1/9}$ and $CD_{1/4}$ could be attributed to amino group (NH_2) [26]. This suggested amino groups of lysine were successfully incorporated into these CDs. As for $CD_{1/9}$, $CD_{1/4}$, $CD_{1/2}$, $CD_{3/4}$, CD_1 and oxalic acid, they all had peak around 1697 cm^{-1} (C=O of oxalic acid) [27]. This indicated incorporation of functional groups of oxalic acid into these CDs. CD_0, $CD_{1/9}$, $CD_{1/4}$ and $CD_{1/2}$ showed a specific characteristic peak at 1579 cm^{-1}, which could be assigned to amide II vibration [28].

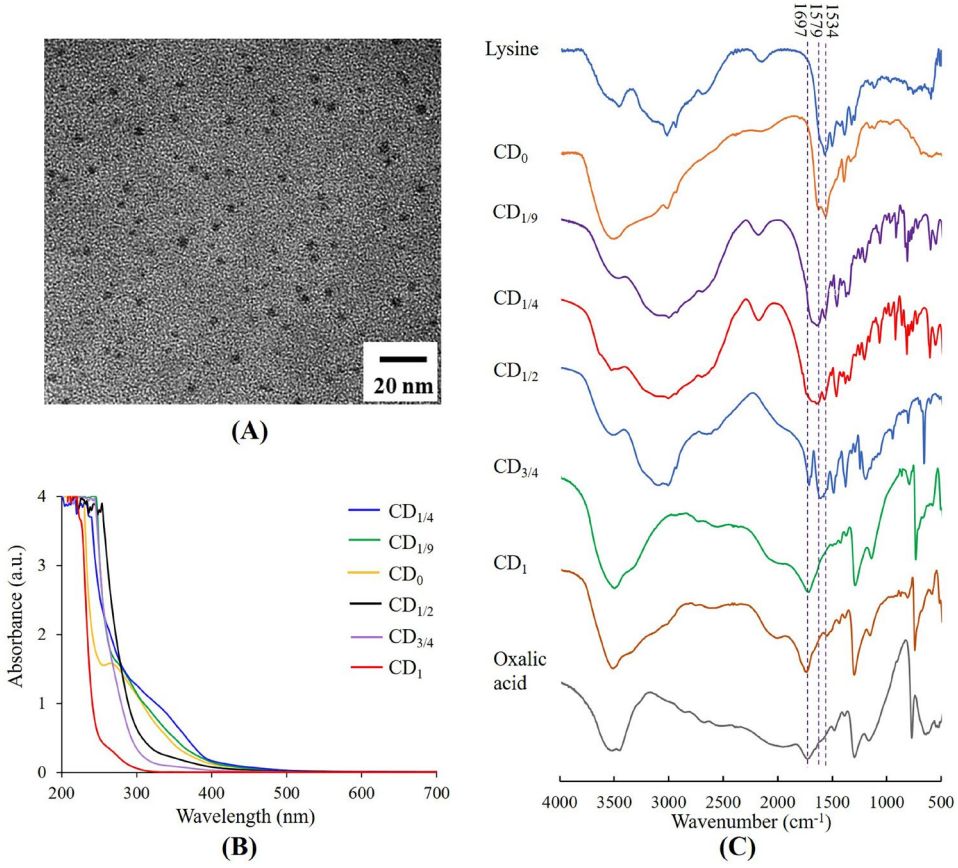

Fig. 1 Characterization of CDs. (**A**) TEM image of $CD_{1/4}$, (**B**) UV–vis spectra, (**C**) FTIR spectra

The XPS spectra revealed three predominant peaks at 285.9, 400.1 and 531.3 eV, which corresponded to binding energies of C 1s, N 1s and O 1s respectively (Fig. 2A-F). CD_0, $CD_{1/9}$, $CD_{1/4}$, $CD_{1/2}$ and $CD_{3/4}$ contained the same elements, except for CD_1. There was no N-compound in staring materials of CD_1, which caused absence of nitrogen. High resolution of the C 1s spectrum could be divided into four binding energy subpeaks (Fig. 2G-L), which included 284.5 eV (C=C/C-C), 285.9 eV (C–N/C-O), 287.9 eV (C=O) and 288.7 eV (O=C-O/O=C-N), respectively [28–31]. From the spectra, it could be seen that the C=C/C-C component had the most intense peak among all of the deconvoluted peaks, indicating that C=C/C-C was the main C bonding configuration of CDs. The peak at 288.7 eV increased from 3.73 to 22.43% with the increasing ratio of oxalic acid in starting materials (Table S2). This could be attributed to carboxylation by oxalic acid and/or conjugation of oxalic acid to amino groups through amide bonds [31]. The N 1s spectrum (Fig. 2M-Q) can be de-convoluted into two peaks at 400.8 and 399.2 eV, corresponding to the N-$(C)_3$ and N-H, respectively [30, 32]. The contents of N-H in CD_0, $CD_{1/9}$ and $CD_{1/4}$ were relatively high, while its contents in $CD_{1/2}$ and $CD_{3/4}$ were quite low (Table S3). This indicated nearly all of the N element in lysine was converted into N-$(C)_3$ when high amounts of oxalic acid were added.

When low amounts of oxalic acid were added in starting materials, the yields of CD_0, $CD_{1/9}$ and $CD_{1/4}$ were above 92% (Fig. 2R). As the oxalic acid content continued to increase, the yield decreased sharply in $CD_{1/2}$, $CD_{3/4}$ and CD_1. This decreasing could be attributed to decarboxylation reaction of oxalate ester [31]. Combining the results of FTIR, XPS and production yields, it can be inferred that oxalic acid was conjugated on the surface of CDs through amide bond in $CD_{1/9}$ and $CD_{1/4}$, through ester bond in $CD_{3/4}$ and CD_1, through amide and ester bonds in $CD_{1/2}$.

Gel-sol transition of different metal-alginate hydrogels

Ca-hydrogel was totally dissolved by $CD_{1/4}$ within 25 min, however, other metal-hydrogels were only partially dissolved (Fig. 3A, B and E*)*. Figure 3C and D showed only Ca^{2+} caused precipitation after reacting with $CD_{1/4}$, suggesting the action mode of Ca^{2+} differed from other metal ions. Fluorescence spectrum (Fig. 3F) revealed decreasing fluorescence intensity of $CD_{1/4}$ after incubating with metal ions except for Ca^{2+}. According to previous reports, Cu^{2+}, Zn^{2+}, Fe^{3+} and Al^{3+} tend to form

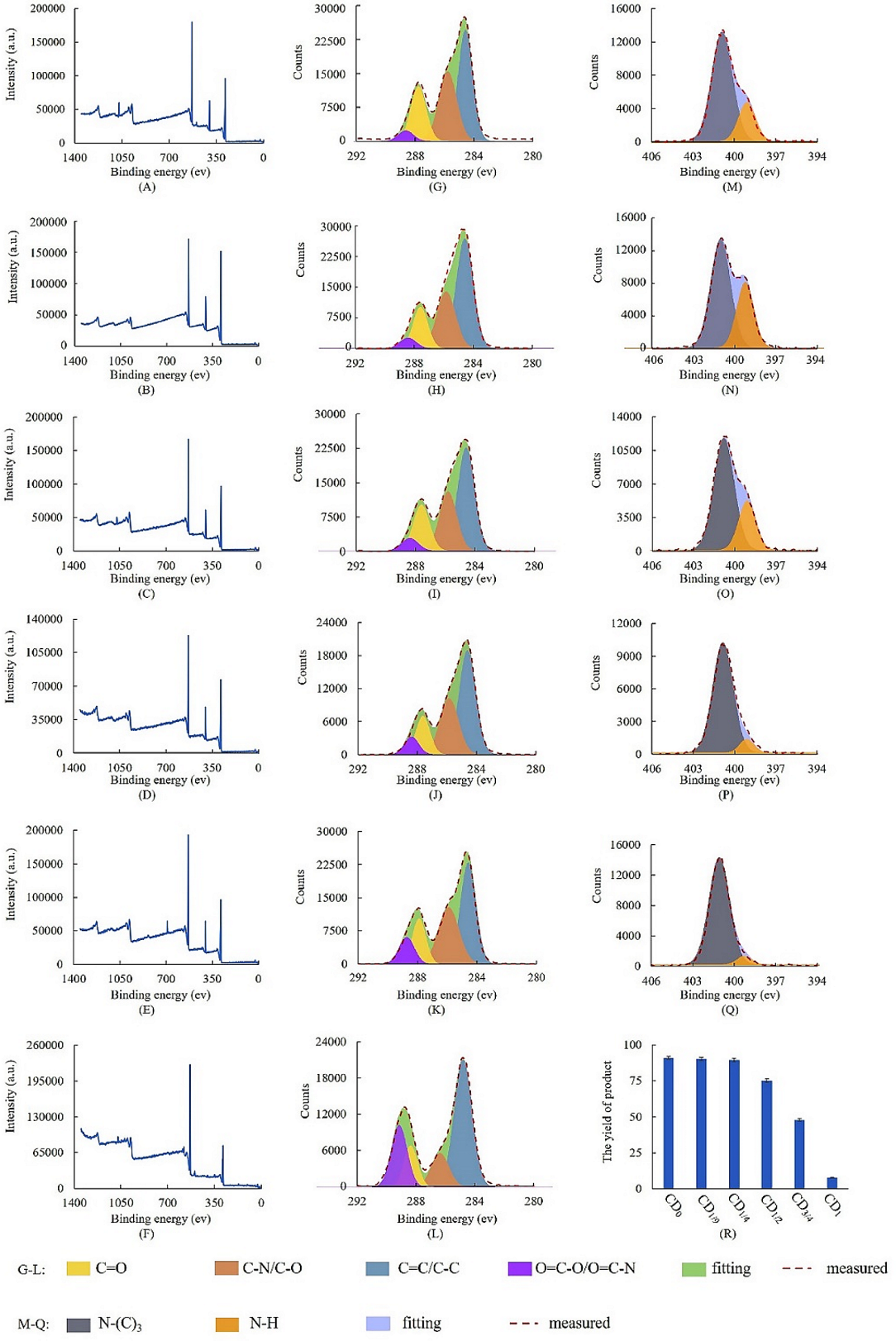

Fig. 2 XPS spectra of CDs. XPS full spectra of (**A**) CD_0, (**B**) $CD_{1/9}$, (**C**) $CD_{1/4}$, (**D**) $CD_{1/2}$, (**E**) $CD_{3/4}$ and (**F**) CD_1; C 1s spectra of (**G**) CD_0, (**H**) $CD_{1/9}$, (**I**) $CD_{1/4}$, (**J**) $CD_{1/2}$, (**K**) $CD_{3/4}$ and (**L**) CD_1; N 1s spectra of (**M**) CD_0, (**N**) $CD_{1/9}$, (**O**) $CD_{1/4}$, (**P**) $CD_{1/2}$, and (**Q**) $CD_{3/4}$; (**R**) the yield of products

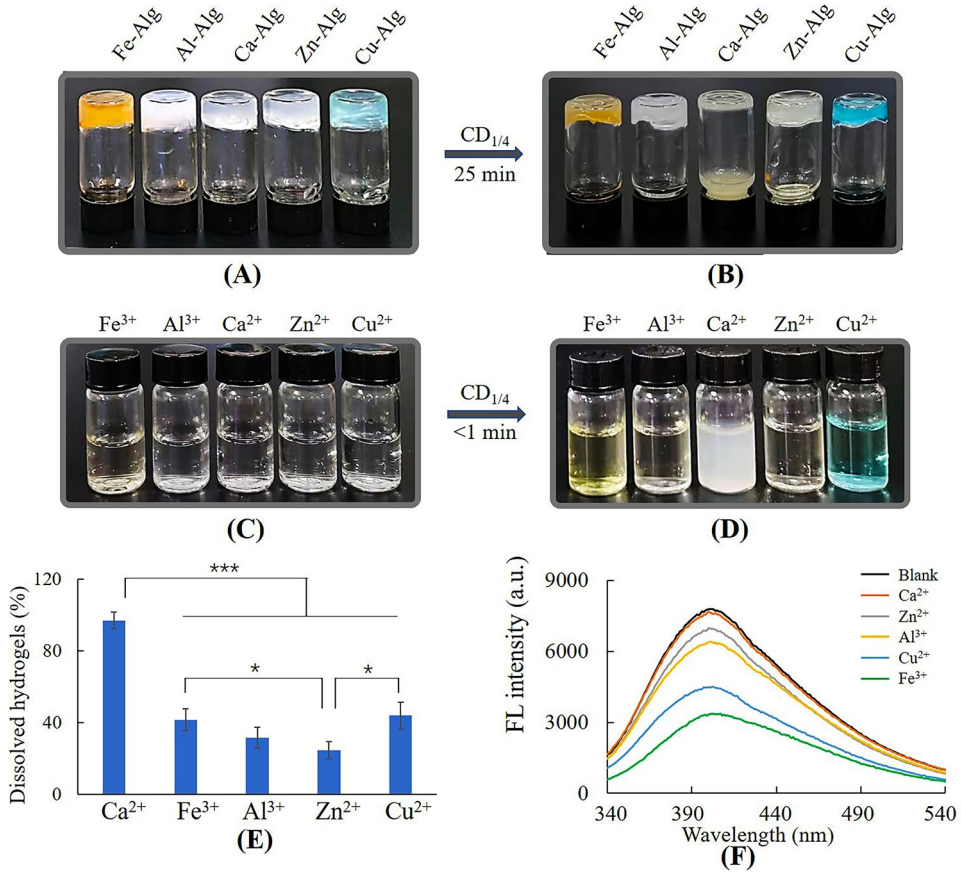

Fig. 3 Dissolution of metal-alginate hydrogels by $CD_{1/4}$. (**A**) Metal-alginate hydrogels, (**B**) metal-alginate hydrogels dissolved by 50 mg/mL $CD_{1/4}$, (**C**) 2.5 mL of 3 mM metal ion solution, (**D**) metal ion solution added with $CD_{1/4}$ (0.8 mL, 50 mg/mL), (**E**) the ratio of dissolved hydrogels, (**F**) fluorescence intensity of 0.48 mg/mL $CD_{1/4}$ with 0.1 mM metal ions

metal complexes with functional groups such as amino and carboxylic groups [33–36], and the static quenching was due to formation of non-fluorescent complexes between $CD_{1/4}$ and these metal ions [29, 37]. The dissolution of these metal-alginate hydrogels could be attributed to the competitive complexation of CDs with Cu^{2+}, Zn^{2+}, Fe^{3+} or Al^{3+} [18]. As for Ca^{2+}, it is much harder to form metal complexes due to the lack of preferred geometrical coordination and coordination numbers, resulting from its large ionic radii and electronic configuration [38]. Thus, gel-sol transition mechanism of Ca-alginate hydrogel can't be attributed to competitive complexation, but may be related to formation of white calcium precipitations. The details were investigated in the following studies.

Effect of amino groups of CDs on gel-sol transition

Figure 4A-D showed that $CD_{1/9}$ and $CD_{1/4}$ aqueous solutions could produce precipitates with Ca^{2+} and dissolve Ca-alginate hydrogels. $CD_{1/2}$, $CD_{3/4}$ and CD_1 aqueous solutions could produce precipitates with Ca^{2+}, but can't dissolve Ca-alginate hydrogels. When the mass fraction of OA in starting materials was ≤1/4, the dissolving ratio of CD_{Lys} increased with the increasing of OA content. When the mass fraction of OA was >1/4, CD_{Lys} lost their ability to dissolve Ca-alginate hydrogels. To clarify the differences between dissolved hydrogel and undissolved hydrogel, SEM and XRD were used to investigate the hydrogels and precipitations. $CD_{1/4}$ was chosen as the research model due to the fastest-dissolving rate, and $CD_{3/4}$ without any dissolution ability was used as a comparison. It was observed by SEM that Ca-alginate hydrogel without any treatment had smooth surface structures (Fig. 4E). After treating with $CD_{3/4}$ for 15 min, the hydrogel had a very coarse surface constituting of countless microparticles (Fig. 4G and H). EDS mapping in Fig. 4I demonstrated Ca-alginate hydrogel treated with $CD_{3/4}$ was entirely covered with calcium. XRD spectra in Fig. 4N showed characteristic peaks at 14.9 and 24.5, which were the same to calcium oxalate crystals [39]. These results indicated mineralization of $CD_{3/4}$ into Ca-alginate hydrogels.

After treating with $CD_{1/4}$ for 15 min, some clusters with different sizes were depositing on remaining hydrogels (Fig. 4F and J). EDS mapping of calcium revealed low enrichment of calcium on small clusters (red arrows) and

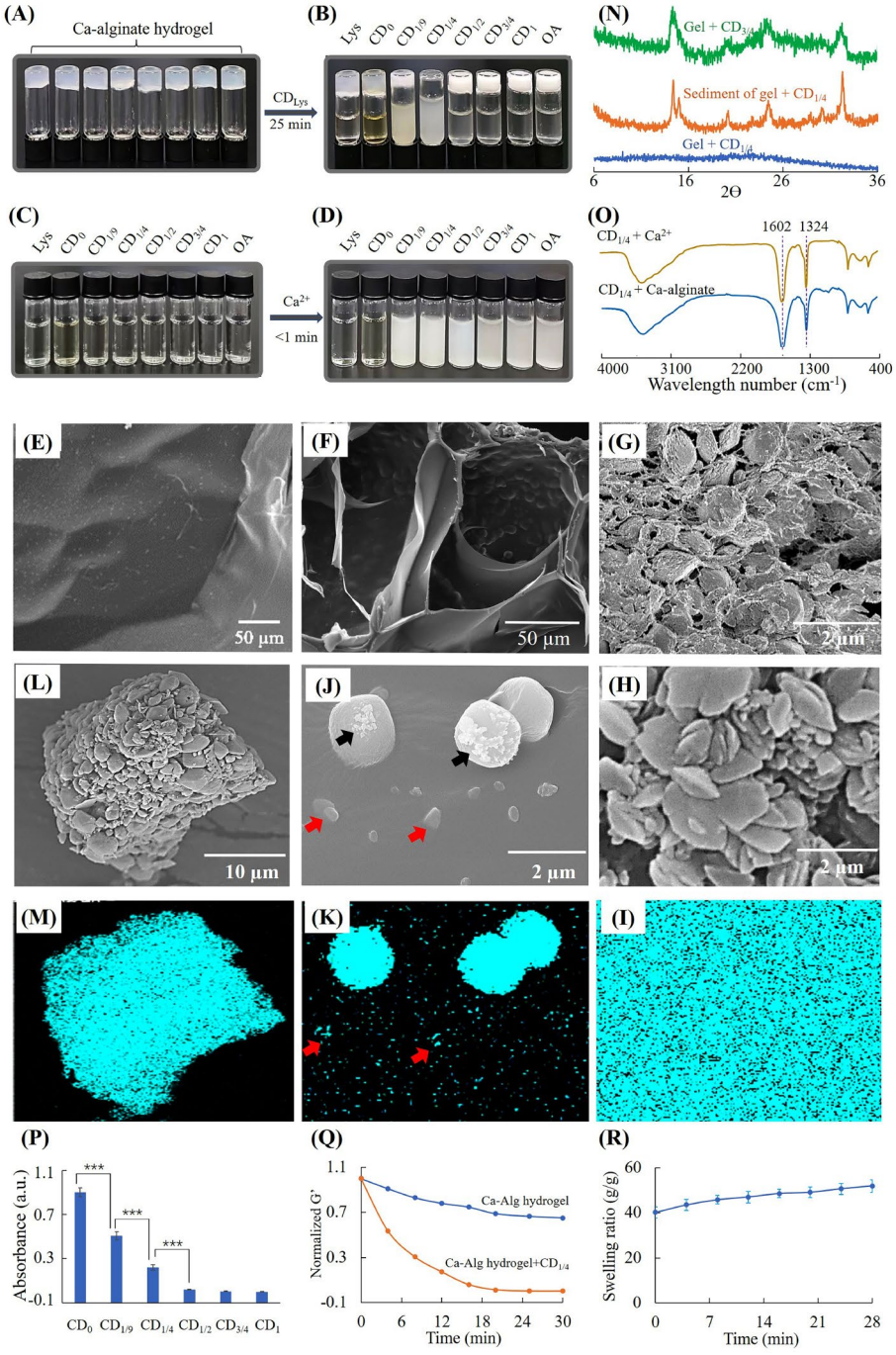

Fig. 4 Dissolution of Ca-alginate hydrogel by CD_{lys}. (**A**) Ca-alginate hydrogel, (**B**) Ca-alginate hydrogel incubated with 18 mg/mL CD_{Lys}, (**C**) 18 mg/mL CD_{lys}, (**D**) CD_{Lys} added with Ca^{2+} (final concentration 3mM), (**E**) surface morphology of Ca-alginate hydrogel, (**F**) cross section morphology of Ca-alginate hydrogel treated with $CD_{1/4}$ for 15 min, (**G**) cross section morphology of Ca-alginate hydrogel treated with $CD_{3/4}$ for 15 min, (**H**) morphology and (**I**) EDS mapping of surface of Ca-alginate hydrogel treated with $CD_{3/4}$ for 15 min, (**J**) morphology and (**K**) EDS mapping of surface of Ca-alginate hydrogel treated with $CD_{1/4}$ for 15 min, (**L**) morphology and (**M**) EDS mapping of centrifugal precipitation of Ca-alginate hydrogel treated with $CD_{1/4}$, (**N**) XRD spectra, (**O**) FTIR of calcium precipitations, (**P**) absorption of CD_{lys} solutions from ninhydrin tests, (**Q**) rheological analysis and (**R**) swelling of hydrogel during degradation by $CD_{1/4}$ solutions

high enrichment of calcium on large clusters (Fig. 4J and K). Irregular shaped crystals (black arrows) also could be seen on part of large clusters, which suggested the occurrence of mineralization. In order to further investigate the fate of calcium crystals, the suspension after gel-sol transition was centrifugated and separated. Figure 4L and M showed EDS map of calcium was totally matched with centrifugal precipitations. XRD spectra of centrifugal

precipitations showed the same peaks as calcium oxalate crystals [39], while remaining hydrogel had no such characteristic peaks. It could be inferred that calcium crystals were finally release to surrounding solutions.

In order to investigate whether alginate participated in mineralization of $CD_{1/4}$, the suspension after gel-sol transition was separated by centrifugation and measured by FTIR. As shown in Fig. 4O, the spectrum of sediment separated from hydrogel suspension was the same as that of sediment generated by $CD_{1/4}$ and Ca^{2+}. Both of them had peaks at 1602 and 1324 cm^{-1}, which could be attributed to amide II vibration and C-O stretching vibration of calcium precipitation, respectively [40]. Figure S3 showed the spectrum of pure SA was similar to that of supernatant separated from the dissolved Ca-alginate hydrogel. Both of them had peaks at 1613, 1413 and 1031 cm^{-1}, which were assigned to antisymmetric COO^- stretch, symmetric COO^- stretch and antisymmetric C-O-C stretch of SA, respectively [41]. The peak at 1525 could be assigned to unreacted amino groups in $CD_{1/4}$. Thus, it could be inferred that alginate did not involve in formation of calcium precipitation and was released to surrounding solution.

As primary amine groups have high binding capacity to carboxyl groups, the amount of primary amine groups on CDs was measured by the ninhydrin reaction. Figure 4P showed the amounts of primary amine groups reduced rapidly with the increasing of oxalic acid. When the content of oxalic acid in starting materials increased to 50%, there was barely no primary amine group on the surface of CD_{Lys}. Figure 4Q showed the storage modulus of hydrogel decreased with time, indicating the hydrogel dissolved progressively. Figure 4R showed the Ca-alginate hydrogel swelled during dissolution of by $CD_{1/4}$. The swelling of hydrogels could be attributed to two reason; ① displacement of cross-linking Ca^{2+} by amino groups, ② capture of Ca^{2+} by CDs [42]. These render the Ca-alginate hydrogel structure loose and soluble.

Effect of different N-groups on surface of CDs on gel-sol transition

To re-verify whether primary amine groups could avoid mineralization of alginate, serine (neutral amino acids) and aspartate (acidic amino acid) with similar molecular weight to lysine (alkaline amino acids) were chosen as the starting materials for preparation of CDs. CD_{Lys}, CD_{Asp} and CD_{Ser} all produced precipitate with Ca^{2+}, however, only CD_{lys} could dissolve Ca-alginate hydrogels (Figure 5A-C). Figure5D showed there was little primary amine group in CD_{Ser} and CD_{Asp}. This test further verified CDs with large amounts of primary amine groups could avoid mineralization of alginates and promote gel-sol transition of Ca-alginate hydrogel. Otherwise, CDs with little amounts of primary amine groups on the surface couldn't avoid mineralization of alginates, which blocked the gel-sol transition.

In order to investigate whether other N-groups on surface of CDs could promote dissolution of Ca-alginate hydrogels, PEI, His, Arg and Pro were chosen as the starting materials for preparation of CDs. Figure 5E-G showed that all of these CDs could generate precipitates with Ca^{2+}, however, the dissolving rate was different from each other. Ninhydrin test and FTIR were used to characterize the N-groups. The ninhydrin reactions of $CD_{1/4+His}$, $CD_{1/4+Arg,}$ $CD_{1/4+PEI}$ and $CD_{1/4+Pro}$ were negative, indicating absence of primary amine groups (Fig. 5H). As shown in Fig. 5I, the peak at 1516 cm^{-1} in CD_{PEI} could be assigned to secondary amine groups. The peak at 1348 cm^{-1} in CD_{His} and CD_{Arg} could be assigned to C-N of secondary amine in histidine/arginine. Figure 5G showed hydrogels treated with CD_{His} or CD_{Arg} for 60 min were completely dissolved, although the dissolving rate were slower than that of CD_{Lys}. The dissolution could be ascribed to the presence of secondary amine groups in CD_{His}/CD_{Arg}, which forms H bond with carboxyl in alginates. Figure 5G and J showed hydrogel treated with CD_{Pro} was hardly dissolved and turned from transparent to white, indicating mineralization of CD_{Pro}-treated hydrogel. It also can be seen that hydrogel treated with CD_{PEI} was partially dissolved and turned from transparent to white eventually. The dissolution could be ascribed to the presence of secondary amine groups in CD_{PEI}. After running out of secondary amine groups, the mineralization occurred on alginate and blocked gel-sol transition. In all, primary and secondary amine groups on surface of CDs could promote dissolution of Ca-alginate hydrogels, and $CD_{1/4}$ baring primary amine groups is the most effective.

In vitro cytotoxicity

As shown in Fig. 6A, oxalic acid exhibited very high cytotoxicity even at the concentration of 1 mg/mL. Lysine exhibited low cytotoxicity at the concentration higher than 18 mg/mL. The cytotoxicity of lysine disappeared after formation of CD_0 (Fig. 6B), which could be ascribed to the decreasing of solute concentration and osmotic pressure. When the ratio of oxalic acid to lysine was no more than 1/4, CDs showed no cytotoxicity. Otherwise, CDs had extremely high cytotoxicity. In order to investigate the reason of difference in cytotoxicity, formation of mineralized crystals in cells was observed at different conditions. Figure S4 showed there were obvious crystals in $CD_{3/4}$ and CD_1 treated cells. The reason may be that $CD_{3/4}$ and CD_1 didn't have enough primary/secondary amine groups on the surface and subcellular structures were also involved in the mineralization of $CD_{3/4}$/CD_1. Otherwise, the mineralization occurred only on $CD_{1/4}$ without subcellular structures. Figure 6C and D

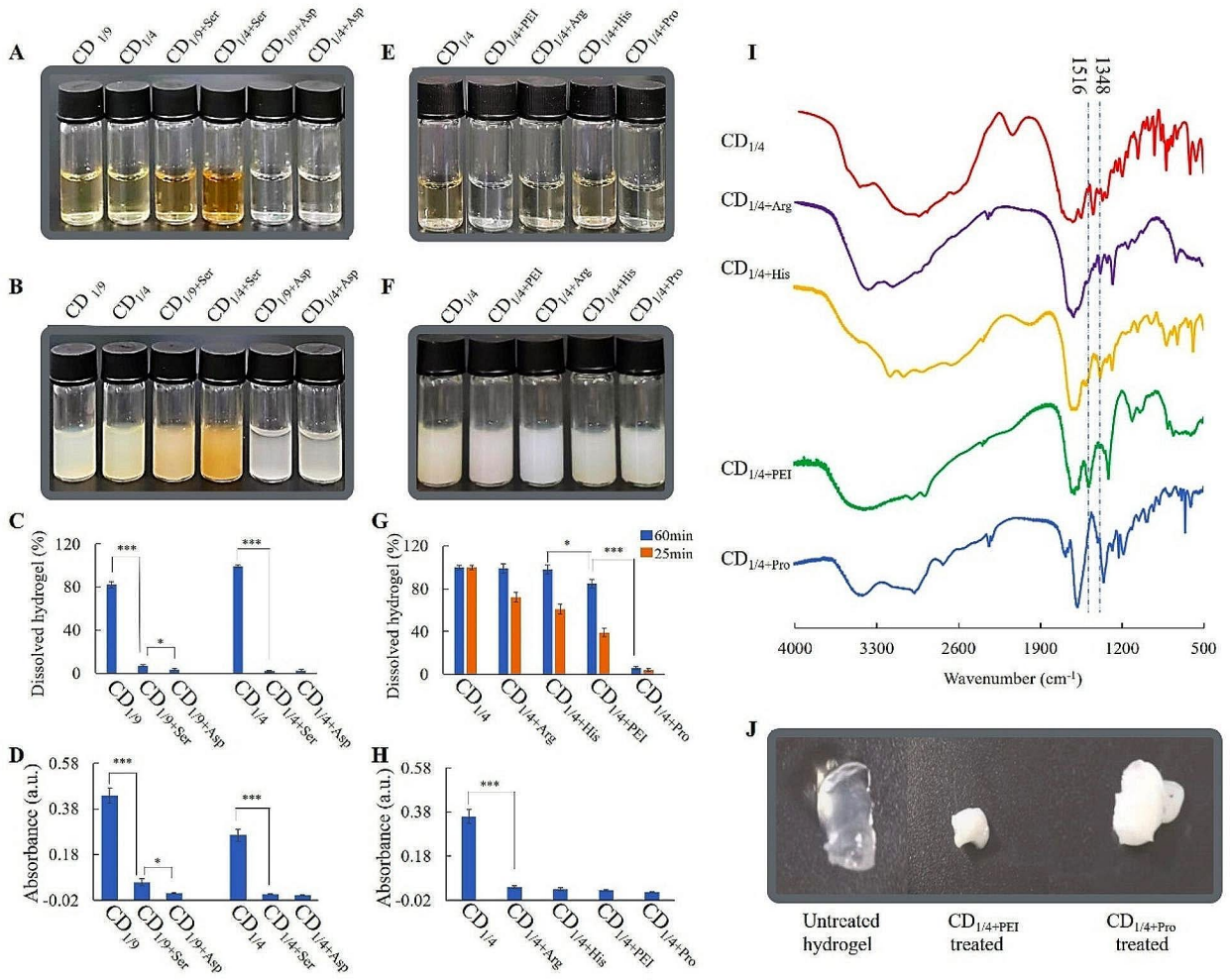

Fig. 5 Dissolution of Ca-alginate hydrogels by CDs with different N-groups. (**A**) 18 mg/mL CD_{Ser}/CD_{Asp} solution, (**B**) CD_{Ser}/CD_{Asp} added with Ca^{2+} (final concentration 3 mM), (**C**) the ratio of dissolved hydrogels treated with CD_{Ser}/CD_{Asp}, (**D**) absorption of CD_{Ser}/CD_{Asp} solutions from ninhydrin tests, (**E**) 18 mg/mL CD_{Arg}/CD_{His}/CD_{Pro}/CD_{PEI} solution, (**F**) CD_{Arg}/CD_{His}/CD_{Pro}/CD_{PEI} added with Ca^{2+} (final concentration 3 mM), (**G**) the ratio of dissolved hydrogels treated with CD_{Arg}/CD_{His}/CD_{Pro}/CD_{PEI}, (**H**) absorption of CD_{Arg}/CD_{His}/CD_{Pro} /CD_{PEI} solutions from ninhydrin tests, (**I**) FTIR spectra of CD_{Arg}/CD_{His}/CD_{Pro}/CD_{PEI}, (**J**) changes in hydrogel treated with $CD_{1/4+PEI}$ and $CD_{1/4+Pro}$

revealed CDs had much lower cell viability than physical mixtures with the same component at same ratio. Physical mixtures even exhibited very high cytotoxicity at low concentration. The reason may be that formation of CDs could reduce the acidity of oxalic acid. In essence, oxalic acid is a strong acid due to the presence of two neighbouring carboxyl groups. One of the carboxyl groups was conjugated to the surface of CDs, which destroyed the structure of neighbouring carboxyl groups. In all, oxalic acid had relatively high cytotoxicity, and its cytotoxicity could be efficiently reduced through forming CDs.

Figure S5 revealed cell viabilities were more than 95% for both hydrogel extract and sol suspension at the concentration of 0.1–10 mg/mL, suggesting good biocompatibility of Ca-alginate hydrogels before and after dissolution

Antimicrobial effect of $CD_{1/4}$ against *E. coli* and *S. aureus*

$CD_{1/4}$ at the concentration of 18 mg/mL was used to treat *E. coli* and *S. aureus*. Figure 6E and F showed the number of *E. coli* and *S. aureus* in the control groups increased continuously in 6 h. But, $CD_{1/4}$ treatment led to decrease in the first hour and slow increase within 2–6 h. These results indicated effectiveness of $CD_{1/4}$ on the inhibition of *E. coli* and *S. aureus*. TEM analysis was carried out to observe morphological changes of *E. coli*. Evenly arranged internal constituents was observed in *E. coli* treated with 3 mg/mL $CD_{1/4}$ (Fig. 6G), while loss of internal constituents was observed in *E. coli* treated with 18 mg/mL $CD_{1/4}$ (Fig. 6H). According to previous reports, oxalic acid can disrupt cell wall integrity by chelating Ca^{2+} in cell walls [43]. Thus, it could be inferred

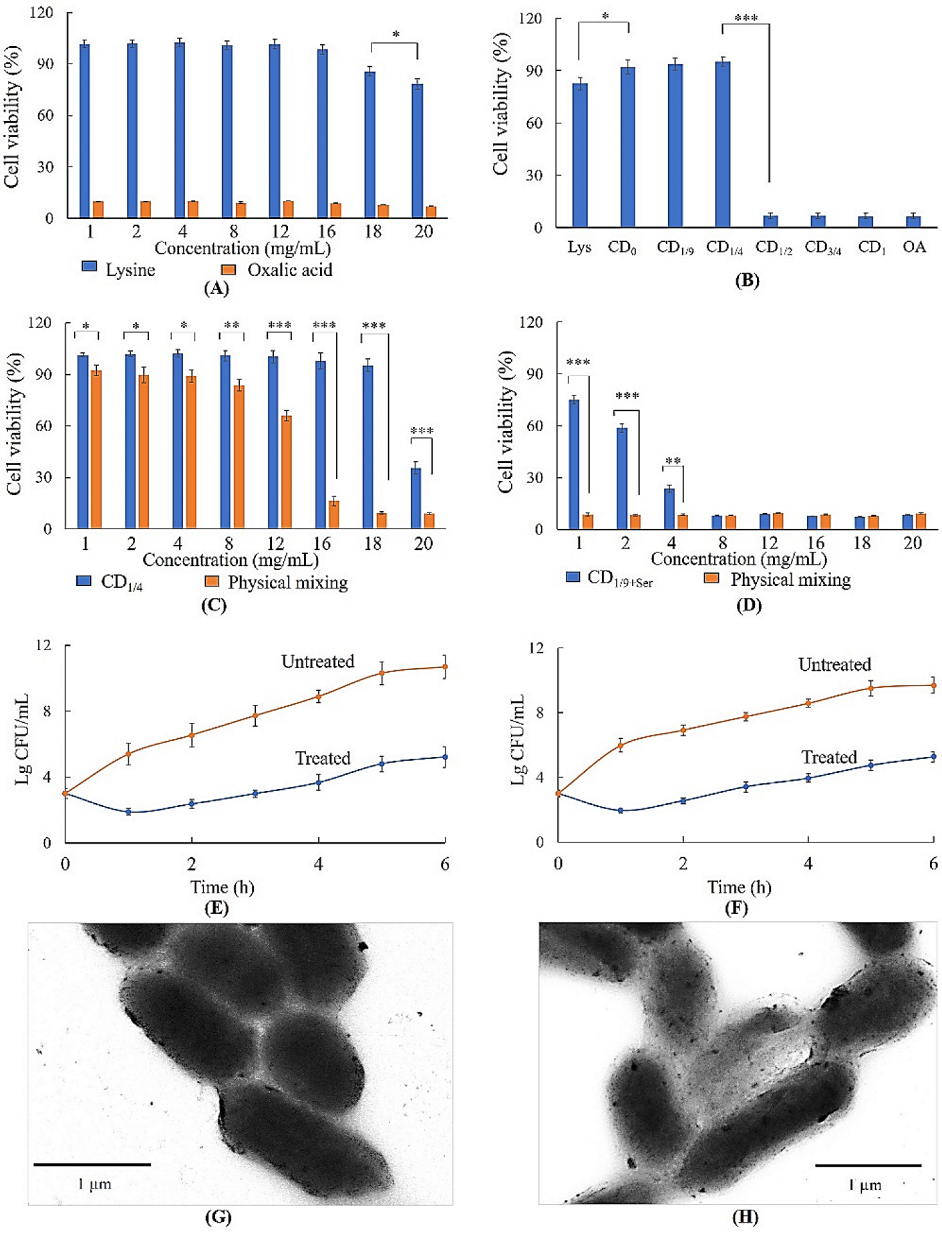

Fig. 6 Cytotoxicity and antibacterial effect of CDs. Cytotoxicity of L929 cells treated with (**A**) starting materials of CDs, (**B**) CD_{lys} at the concentration of 18 mg/mL, (**C**) $CD_{1/4}$, and physical mixture with the same ratio of oxalic acid to lysine and (**D**) $CD_{1/4+Ser}$, and physical mixture with the same ratio of oxalic acid to serine; (**E**) growth curve of *E. coli.* treated with $CD_{1/4}$; (**F**) growth curve of *S. aureus.* treated with $CD_{1/4}$; (**G**) TEM image of *E. coli.* treated with 3 mg/mL $CD_{1/4}$ and (**H**) TEM image of *E. coli.* treated with 18 mg/mL $CD_{1/4}$

that $CD_{1/4}$ exert antimicrobial effect through destroying cell walls.

Burn wound healing effect

The photographs and contraction rate of the burn wounds in different groups from day 1 to day 24 were presented in Fig. 7A and B. Starting from day 12, the wounds treated with dissolving hydrogels were healed significantly faster than control and/or hydrogel groups. The burn wound was almost completely recovered on day 24 in the hydrogel+$CD_{1/4}$ group, whereas visible wounds were still observable in other groups. H&E and Masson trichrome staining were used to assess the histopathological structures of wound tissue from regenerated skin on day 16. As shown in Fig. 7C, there was still epidermal rupture in control group. From Masson's trichrome-stained images, it was observed that wound treated with dissolvable hydrogel produced greatly more collagen than other groups (Fig. 7D). Above outcomes revealed that the Ca-alginate hydrogel with replacement enhanced

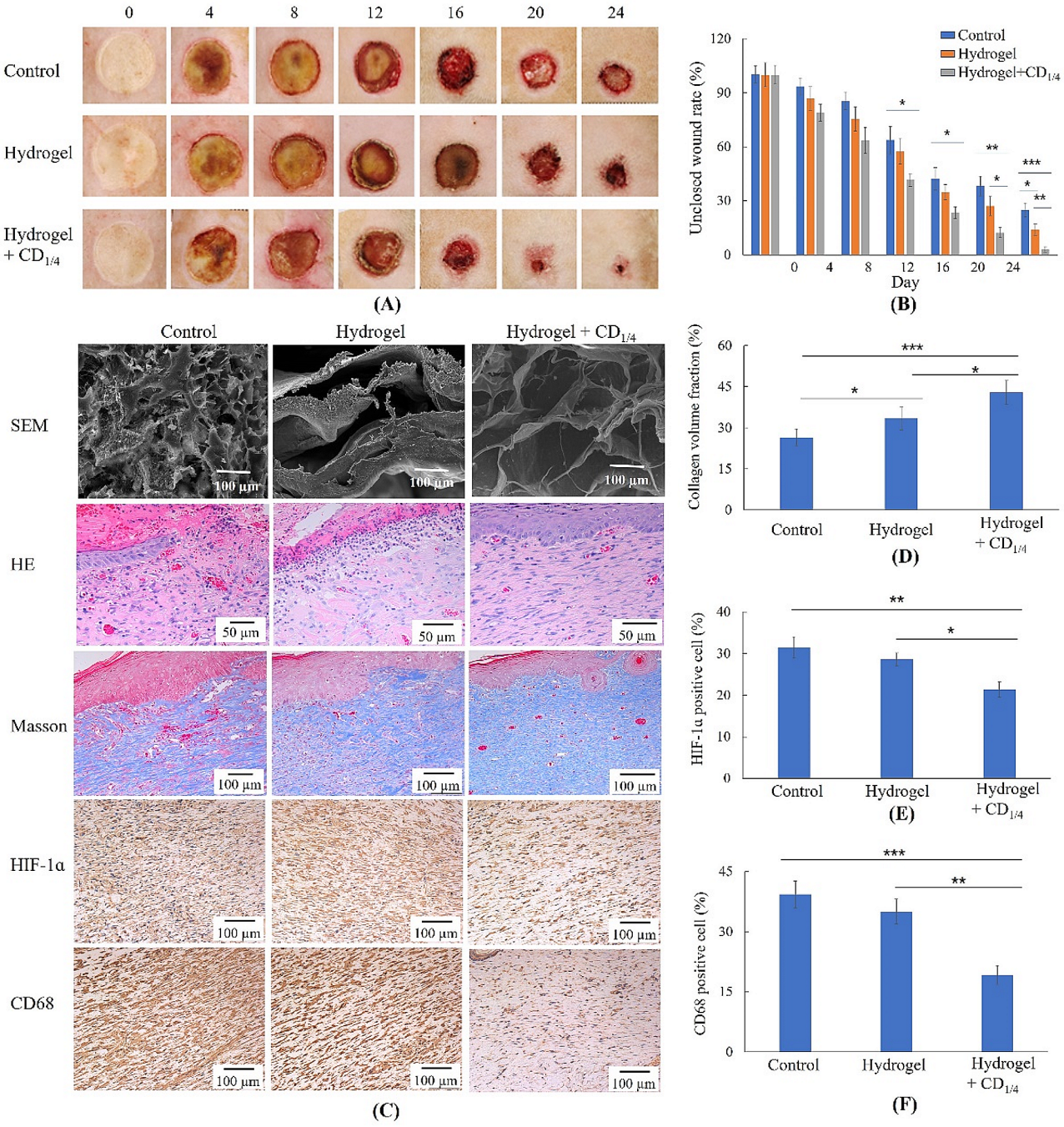

Fig. 7 In vivo wound healing performances. (**A**) Photographs of wounds healed at different time points after various treatments, (**B**) percentage of unhealed wound area, (**C**) SEM, histological and immunohistochemical staining of wound sections, (**D**) percentages of collagen deposition area, (**E**) HIF-1α positive cell density, (**F**) CD68 positive cell density

re-epithelialization and collagen production. SEM images showed the newly formed hydrogels on wounds had porous structures, while the other two groups were nearly nonporous on day 17. The porous structure in hydrogel enables air circulation, oxygen supply and wound exudate absorption during wound healing process [44]. But the exudate wound block the holes of hydrogels [19]. To assess whether Ca-alginate hydrogel with replacement could alleviate hypoxia, new generated tissues were observed by HIF-1α immunostaining (brown cells). The relative HIF-1α expression in the hydrogel+$CD_{1/4}$ group was significantly lower than that in control and hydrogel only groups (Fig. 7E), proving hypoxia relief of replaceable hydrogels. Local inflammation also exerts a key

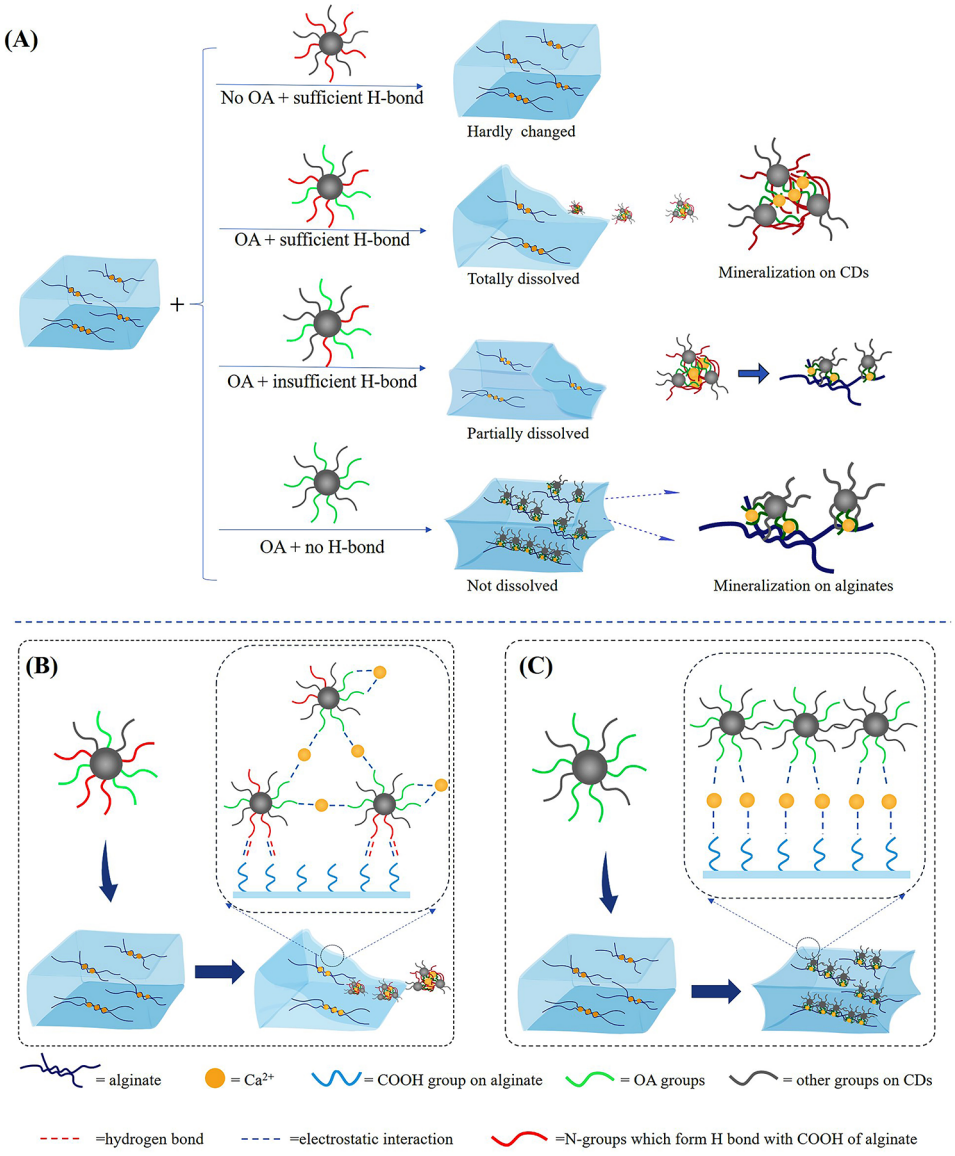

Fig. 8 The role of primary/secondary amine groups in mineralization procedure. (**A**) CDs containing different N-groups on gel-sol transition, (**B**) interaction between Ca-alginate hydrogel and CDs with abundant primary/secondary amine groups on the surface, (**C**) interaction between Ca-alginate hydrogel and CDs with little primary/secondary amine groups on the surface

effect on wound healing. The hydrogel with replacement showed much lower CD68-positive macrophage (brown cells) density than the other two groups (Fig. 7F). These results indicated that dissolvable hydrogel could effectively alleviate local inflammatory reactions. This could be ascribed to the improved oxygen supply of hydrogels and antibacterial properties of CDs. According to previous reports, improved oxygen supply could accelerate the resolution of the initial inflammation phase and the progression of the proliferation phase [45].

Mechanisms and future perspectives

In this work, CDs with primary and secondary amine groups have been prepared for promoting gel-sol transition of Ca-alginate hydrogel *via* site-specific mineralization. The amount of primary/secondary amine groups played key role in determining where mineralization occurred and whether gel-sol transition happened (Fig. 8A). Ca^{2+} bound to carboxyl group through electrostatic interactions. Primary and secondary amine groups bound to carboxyl groups through not only electrostatic interactions but also hydrogen bonds (Fig. 8B and C). Primary and secondary amine groups could compete with Ca^{2+} for binding to carboxyl groups in alginates. Therefore, Ca^{2+} only bound to CDs in case of CDs with large

amounts of primary and secondary amine groups. Considering the role of cooperative ion-association in mineralization process and results in this work [46], the gel-sol transition could be inferred as follows. At first, CDs got close to alginate hydrogel. Ca^{2+} bound to primary and secondary amine groups on CDs and formed small clusters on hydrogels. Ca^{2+} continued to accumulate around CDs, resulting in bigger cluster and formation of calcium crystals. Then, the calcium in hydrogel was transformed to calcium crystals and released into surrounding solutions at last. But if there were not sufficient primary/secondary amine groups on CDs, the Ca^{2+} bound to both CDs and alginates. This caused mineralization of both CDs and alginates, thereby blocking dissolution of alginate hydrogel.

Our results also demonstrated CDs prepared from oxalic acid had much less cytotoxicity than oxalic acid. In essence, oxalic acid is a strong acid due to the presence of two neighbouring carboxyl groups. Formation of CDs could reduce the cytotoxicity of oxalic acid through destroying the structure of neighborly carboxyl groups and decreasing the acidity of oxalic acid. Moreover, mineralization of calcium oxalate could occur on the subcellular structures and destroy homeostasis of physiologic functions. The abundant primary/secondary amine groups on CDs could reduce the cytotoxicity of oxalic acid through avoiding mineralization of subcellular structures. In all, the cytotoxicity of oxalic acid could be reduced by two ways: combination with compounds containing primary/secondary amine groups to reduce mineralization on subcellular structures, and formation of CDs to reduce the acidity of oxalic acid.

Adequate oxygen supply has been considered as an efficient strategy for promoting wound healing. Previous reports have proven hyperbaric oxygen therapy and oxygen-releasing system as effective strategies for relieving hypoxia in acute wound, diabetic chronic wound and skin flap transplantation [44, 45, 47–49]. Our groups demonstrated replaceable alginate hydrogel was also an efficient strategy for hypoxia relief. The replaceable hydrogels could form new hydrogels with porous structures, which enhance permeability of hydrogels. Without adding any functional molecules or materials in alginate hydrogel, it has already shown excellent functions in relieving hypoxia and promoting wound healing.

Dissolvable hydrogels have shown much potential in providing easy wound dressing replacement, avoiding mechanical and surgical debridement, and promoting wound healing. In future studies, the dissolvable Ca-alginate hydrogels may be combined with other functional materials and molecules for additional features. The dissolvable hydrogels may be further used to treat refractory wounds such as pressure ulcers, venous ulcers and diabetic wounds. Dissolvable Ca-alginate hydrogel may also be utilized in wearable biosensors, for it could be facilely removed from tissues whenever necessary. The main limitation of CDs for dissolving Ca-alginate hydrogel through mineralization method lies in the limited dissolution rate. In order to accelerate the dissolving rate, template molecules that have higher association ability with carboxyl groups on alginates may be used as starting materials for CDs.

Conclusions

We developed an appealing paradigm of gel-sol transition that was facilitated by CDs *via* site-specific mineralization. The amount of primary/secondary amine groups on CDs played key role during gel-sol transition. On the one hand, these N-groups on surface of CDs could form H-bond with carboxyl groups and compete with Ca^{2+} for carboxyl groups of alginates. This could block mineralization of alginates and promote gel-sol transition. On the other hand, CDs with N-groups also could act as templates for mineralization, which promoted seizing Ca^{2+} from Ca-alginate hydrogels. Moreover, CDs possessed antibacterial activity through seizing Ca^{2+} from cell walls, and the renewed porous hydrogels could relieve hypoxia in wound area. This work highlights the gel-sol transition of Ca-alginate hydrogels through site-specific mineralization of CDs, the role of primary/secondary amine groups on CDs and successful treatment of burn wound.

Supplementary Information

The online version contains supplementary material available at https://doi.org/10.1186/s12951-024-02729-5.

Supplementary Material 1

Acknowledgements
The authors gratefully acknowledge the financial supports from the Natural Science Foundation of Shandong Province (ZR2020MH324).

Author contributions
Q.L. designed the whole study, carried out the original draft and provided financial support. C.L. and D.X. helped with the animal experiment and reviewed the manuscript.

Funding
This work was supported by the Natural Science Foundation of Shandong Province (ZR2020MH324).

Data availability
No datasets were generated or analysed during the current study.

Declarations

Ethics approval and consent to participate
All animal experiments were approved by the Institutional Animal Care and Use Committee of Affiliated Hospital of Qingdao University.

Consent for publication
All authors have consented to the publication of this article.

Competing interests
The authors declare no competing interests.

Author details
[1]Cancer Institute, The Affiliated Hospital of Qingdao University, Qingdao University, Qingdao 266071, China
[2]College of Marine Life Science, Ocean University of China, Qingdao 266003, China
[3]Qingdao Cancer Institute, Qingdao 266071, China
[4]School of Life Sciences, Tsinghua University, Beijing 100084, China

Received: 12 February 2024 / Accepted: 21 July 2024
Published online: 02 August 2024

References

1. Cai CY, Meng ZJ, Zhao LL, Wu T, Xu X, Zhu YS. A self-assembled peptide hydrogel for wound repair. J Mater Sci. 2022;57:1345–61.
2. Cook KA, Naguib N, Kirsch J, Hohl K, Colby AH, Sheridan R, Rodriguez EK, Nazarian A, Grinstaff MW. In situ gelling and dissolvable hydrogels for use as on-demand wound dressings for burns. Biomater Sci. 2021;9:6842–50.
3. Rade PP, Garnaik B. Ofloxacin-loaded PLLA nanofibrous mats for wound dressing applications. ACS Appl Bio Mater. 2020;3:6648–60.
4. Xu W, Song Q, Xu JF, Serpe MJ, Zhang X. Supramolecular hydrogels fabricated from supramonomers: a novel wound dressing material. ACS Appl Mater Interfaces. 2017;9:11368–72.
5. Gokaltun AA, Fan L, Mazzaferro L, Byrne D, Yarmush ML, Dai T, Asatekin A, Usta OB. Supramolecular hybrid hydrogels as rapidly on-demand dissoluble, self-healing, and biocompatible burn dressings. Bioact Mater. 2023;25:415–29.
6. Xie T, Ding J, Han XX, Jia HZ, Yang Y, Liang S, Wang WX, Liu WG, Wang W. Wound dressing change facilitated by spraying zinc ions. Mater Horiz. 2020;7:605–14.
7. Yan Y, Zhang X, Ren K, Xiao C. On-demand dissolvable hydrogel dressings for promoting wound healing. J Polym Sci. 2024;7:21.
8. Shi J, Wang D, Wang H, Yang X, Gu S, Wang Y, Chen Z, Chen Y, Gao J, Yu L, Ding J. An injectable hemostatic PEG-based hydrogel with on-demand dissolution features for emergency care. Acta Biomater. 2022;145:106–21.
9. Yang Y, Xu H, Li M, Li Z, Zhang H, Guo B, Zhang J. Antibacterial conductive UV-blocking adhesion hydrogel dressing with mild on-demand removability accelerated drug-resistant bacteria-infected wound healing. ACS Appl Mater Interfaces. 2022;14:41726–41.
10. Xu X, Lu W, Zhu J, Pan X, Zhu X. An on-demand dissoluble chitosan hydrogel containing dynamic diselenide bond. Gels. 2021;7:21.
11. Zong Q, Peng X, Ding Y, Wu H, Lu C, Ye J, Sun W, Zhang J, Zhai Y. Multi-functional hydrogel wound dressing with rapid on-demand degradation property based on aliphatic polycarbonate and chitosan. Int J Biol Macromol. 2023;244:125138.
12. Lu H, Yuan L, Yu X, Wu C, He D, Deng J. Recent advances of on-demand dissolution of hydrogel dressings. Burns Trauma. 2018;6:35.
13. Konieczynska MD, Grinstaff MW. On-demand dissolution of chemically cross-linked hydrogels. Acc Chem Res. 2017;50:151–60.
14. Li Q, Liu CG, Huang ZH, Xue FF. Preparation and characterization of nanoparticles based on hydrophobic alginate derivative as carriers for sustained release of vitamin D_3. J Agric Food Chem. 2011;59:1962–7.
15. Hassani MS, Salehi M, Ehterami A, Mahami S, Bitaraf FS, Rahmati M. Evaluation of collagen type I and III, TGF-β1, and VEGF gene expression in rat skin wound healing treated by alginate/chitosan hydrogel containing crocetin. Biochem Eng J. 2023;195:108895.
16. Mao G, Tian S, Shi Y, Yang J, Li H, Tang H, Yang W. Preparation and evaluation of a novel alginate-arginine-zinc ion hydrogel film for skin wound healing. Carbohyd Poly. 2023;311:120757.
17. Khaliq T, Sohail M, Minhas MU, Mahmood A, Munir A, Qalawlus AHM, Jabeen N, Kousar M, Anwar Z. Hyaluronic acid/alginate-based biomimetic hydrogel membranes for accelerated diabetic wound repair. Int J Pharmaceut. 2023;643:123244.
18. Li Q, Shen X, Liu C, Xing D. Facile wound dressing replacement: Carbon dots for dissolving alginate hydrogels via competitive complexation. Int J Biol Macromol. 2023;240:124455.
19. Zeng J, Geng W, Tang Y, Xiong XC, Zhu YJ. Flexible photothermal biopaper comprising Cu2+-doped ultralong hydroxyapatite nanowires and black phosphorus nanosheets for accelerated healing of infected wound. Chem Eng J. 2022;437:135347.
20. Štajner L, Kontrec J, Njegić Dzakula B, Maltar-Strmečki N, Plodiec M, Lyons D, Kralj D. The effect of different amino acids on spontaneous precipitation of calcium carbonate polymorphs. J Cryst Growth. 2018;486:71–81.
21. Weiner S, Addadi L. Crystallization pathways in biomineralization. Annu Rev Mater Res. 2011;41:21–40.
22. Feng ZQ, Yang TY, Liang TT, Wu ZY, Wu T, Zhang JB, Yu L. Biomineralization of calcium carbonate under amino acid carbon dots and its application in bioimaging. Mater Des. 2022;217:110644.
23. Tang XP, Liu X, Hou Y, Cai L, Chen LJ, Wu QH, Yi J, Zhang GL. Various concentrations of carbon nanodots induced fluorescent calcite with multi-morphologies. Cryst Growth Des. 2018;18:6559–63.
24. Guo S, Yang M, Chen M, Zhang J, Liu K, Ye L, Gu W. Bioinspired synthesis of fluorescent calcium carbonate/carbon dot hybrid composites. Dalton Trans. 2015;44:8232–7.
25. Gong X, Lu W, Paau MC, Hu Q, Wu X, Shuang S, Dong C, Choi MM. Facile synthesis of nitrogen-doped carbon dots for Fe(3+) sensing and cellular imaging. Anal Chim Acta. 2015;861:74–84.
26. Boonsongrit Y, Mueller BW, Mitrevej A. Characterization of drug-chitosan interaction by 1H NMR, FTIR and isothermal titration calorimetry. Eur J Pharm Biopharm. 2008;69:388–95.
27. Mitra T, Sailakshmi G, Gnanamani A, Mandal AB. Di-carboxylic acid cross-linking interactions improves thermal stability and mechanical strength of reconstituted type I collagen. J Therm Anal Calorim. 2011;105:325–30.
28. Tian BB, Zheng J, Zhao CX, Liu CB, Su CL, Tang W, Li X, Ning GH. Carbonyl-based polyimide and polyquinoneimide for potassium-ion batteries. J Mater Chem A. 2019;7:9997–10003.
29. Rong M, Feng Y, Wang Y, Chen X. One-pot solid phase pyrolysis synthesis of nitrogen-doped carbon dots for Fe3 + sensing and bioimaging. Sens Actuat B- Chem. 2017;245:868–74.
30. Li G, Lv N, Bi W, Zhang J, Ni J. Nitrogen-doped carbon dots as a fluorescence probe suitable for sensing Fe3 + under acidic conditions. New J Chem. 2016;40:10213–8.
31. Yang Y, Wang MH, Shi ZY, Xiao RB, Sun XC, Chen Y. Synergistic effect of anion and cation in oxalic acid for graphene surface engineering and its enhanced pseudocapacitance performance. J Alloy Compd. 2021;868:159128.
32. Ghosh S, Ghosh A, Ghosh G, Marjit K, Patra A. Deciphering the relaxation mechanism of red-emitting carbon dots using ultrafast spectroscopy and global target analysis. J Phys Chem Lett. 2021;12:8080–7.
33. Goswami B, Yadav R, Schoo C, Roesky PW. Neutral and cationic enantiopure group 13 iminophosphonamide complexes. Dalton Trans. 2020;49:675–81.
34. Lei Y, Huang Q, Shan S, Lin Y, Zhang A. A stretchable and rapidly self-healable polysiloxane elastomer based on reversible aluminum–amino coordination. New J Chem. 2019;43:17441–5.
35. Rathinam B, Liu BT. Highly efficient probe of dinuclear zinc complex for selective detection of oxalic acid. J Taiwan Inst Chem En. 2021;127:349–56.
36. Togashi T, Nakayama M, Hashimoto A, Ishizaki M, Kanaizuka K, Kurihara M. Solvent-free synthesis of monodisperse Cu nanoparticles by thermal decomposition of an oleylamine-coordinated Cu oxalate complex. Dalton Trans. 2018;47:5342–7.
37. Shi B, Su Y, Zhang L, Huang M, Liu R, Zhao S. Nitrogen and phosphorus co-doped carbon nanodots as a novel fluorescent probe for highly sensitive detection of Fe(3+) in human serum and living cells. ACS Appl Mater Interfaces. 2016;8:10717–25.
38. Finelli A, Herault N, Crochet A, Fromm KM. Compartmentalization of alkaline-earth metals in Salen-type Cu- and Ni-complexes in solution and in the solid state. ACS Omega. 2019;4:10231–42.
39. Trouvé G, Michelin L, Kehrli D, Josien L, Rigolet S, Lebeau B, Gieré R. The multi-analytical characterization of calcium oxalate phytolith crystals from grapevine after treatment with calcination. Crystals. 2023;13:967.
40. Shaltout AA, Dabi MM, Said DA, Allam MA, Ahmed SI. EDXRF, FTIR, and XRD characterization of low calcium oxalate urinary stones collected from arid area. X-Ray Spectrom. 2021;51:214–29.
41. Lawrie G, Keen I, Drew B, Chandler-Temple A, Rintoul L, Fredericks P, Grondahl L. Interactions between alginate and chitosan biopolymers characterized using FTIR and XPS. Biomacromolecules. 2007;8:2533–41.
42. Kim W-T, Chung H, Shin I-S, Yam KL, Chung D. Characterization of calcium alginate and chitosan-treated calcium alginate gel beads entrapping allyl isothiocyanate. Carbohyd Polym. 2008;71:566–73.
43. Monazzah M, Soleimani MJ, Tahmasebi Enferadi S, Rabiei Z. Effects of oxalic acid and culture filtrate of Sclerotinia sclerotiorum on metabolic changes

in sunflower evaluated using FT-IR spectroscopy. J Gen Plant Pathol. 2018;84:2–11.
44. Kang JI, Park KM. Oxygen-supplying syringe to create hyperoxia-inducible hydrogels for in situ tissue regeneration. Biomaterials. 2023;293:121943.
45. Zhang Y, Fang M, Xie W, Zhang YA, Jiang C, Li N, Li L, Tian J, Zhou C. Sprayable alginate hydrogel dressings with oxygen production and exosome loading for the treatment of diabetic wounds. Int J Biol Macromol. 2023;242:125081.
46. Zou Z, Polishchuk I, Bertinetti L, Pokroy B, Politi Y, Fratzl P, Habraken WJEM. Additives influence the phase behavior of calcium carbonate solution by a cooperative ion-association process. J Mater Chem B. 2018;6:449–57.
47. Jakfar S, Lin TC, Chen ZY, Yang IH, Gani BA, Ningsih DS, Kusuma H, Chang CT, Lin FH. A polysaccharide isolated from the herb bletilla striata combined with methylcellulose to form a hydrogel via self-assembly as a wound dressing. Int J Mol Sci. 2022;23:12019.
48. Li Q, Shen X, Liu CG, Xing DM. Facile wound dressing replacement: Carbon dots for dissolving alginate hydrogels via competitive complexation. Int J Biol Macromol. 2023;240:124455.
49. Yuan L, Wu Y, Fang J, Wei XJ, Gu QS, El-Hamshary H, Al-Deyab SS, Morsi Y, Mo XM. Modified alginate and gelatin cross-linked hydrogels for soft tissue adhesive. Artif Cell Nanomed B. 2016;45:76–83.

Publisher's Note

Springer Nature remains neutral with regard to jurisdictional claims in published maps and institutional affiliations.